New Insights into Roughness Applications in Tip Vortex Cavitation Inception Mitigation

33rd Symposium on Naval Hydrodynamics
Osaka, Japan, 18-23 Oct 2020

New Insights into Roughness Applications in Tip Vortex Cavitation Inception Mitigation

Urban Svennberg[1], Abolfazl Asnaghi[2], Robert Gustafsson[1], Rickard E. Bensow[2]

([1] Kongsberg Hydrodynamic Research Centre, Kongsberg Maritime Sweden AB, Kristinehamn, Sweden; [2] Department of Mechanics and Maritime Sciences, Chalmers University of Technology, Sweden)

ABSTRACT

Tip vortex cavitation (TVC) is usually the first type of cavitation that appears on a propeller. Therefore, it is considered as the main cavitation characteristics to avoid in the design procedure of low-noise propellers, where their operating profiles demand very low radiated noise emissions. The current study includes both numerical and experimental analyses of blade surface roughness application in order to mitigate TVC inception. The investigation consists of applying roughness application on a classical benchmark, an elliptical foil, and on a propeller selected from a Kongsberg research series of highly skewed propellers having a low effective tip load.

The numerical simulations are performed on an appropriate grid resolution for tip vortex propagation, at least 32 cells per vortex diameter by using Implicit Large Eddy Simulation (ILES) for unsteady simulations, and RANS using the SST $k-\omega$ model with a curvature correction for steady simulations. Two approaches are considered to include roughness in the numerical simulations: using a rough wall function and resolving the flow around the roughness elements. To minimize the negative effects of the roughness on the propeller performance, the roughness area is optimized by simultaneous consideration of the tip vortex mitigation and performance degradation.

Experimental measurements of the elliptical foil are conducted to support the CFD study at different operating conditions and with different roughness patterns while LDV and high-speed video recordings are used to collect the data. The tested conditions include both cavitating and inception of TV flows on the smooth and roughened foil to provide further insights on the usage of roughness.

For the elliptical foil, it is found that the application of roughness can reduce the cavitation number for cavitation inception, σ_i, by 35 $\%$ while keeping the performance degradation less than 1% compared to the smooth foil condition. The average reduction of the TVC inception number achieved by using roughness on the propeller is around 21% with a performance degradation of around 1.5% compared to the smooth propeller condition.

INTRODUCTION

There is an increasing demand for silent operation of propellers at the same time as lower operational cost and higher efficiency are required. Among different propeller noise sources, cavitation is the most pronounced one (Kuiper 1981, Wijngaarden et al. 2005) and the ship speed that cavitation appears on the propeller is a distinguished threshold where the propeller becomes considerably noisier. Tip vortex cavitation (TVC) is normally the first type of cavitation that appears on a propeller. Therefore, it is considered as an important cavitation characteristics to control in the design procedure of low-noise propellers (Higuchi and Arndt 1989, Vesting et al. 2016, Bosschers 2018).

A tip vortex (TV) flow occurs wherever a flow passes over a lifting wing with a finite span. The pressure difference between the foil surfaces drives the fluid from the high pressure side on one surface to the low pressure side on the other. This makes the flow highly three-dimensional at the tip region creating a vortex pattern (Arndt and Arakeri 1991, Arndt 2002). Even though the basic explanation is simple it results in a complex three-dimensional flow feature composed of very small structures in time and space (Hsiao and Chahine 2005). Cavitation and cavitation inception incorporate even further complexity such as interaction of two-phase flows and mass transfer.

In order to increase cavitation inception speed (CIS), different approaches mainly focusing on weakening the TV have been proposed and tested. Among these approaches, the application of roughness is a promising way (Souders and Platzer 1981, Kruger et al. 2016). Application of roughness on a surface promotes turbulence in boundary layers and consequently affects the tip vortex roll-up. The interaction of vortical structures generated by the roughness elements with the main tip vortex destabilizes the tip vortex (Baily and Tavoularis 2008). If the roughness elements properties, such as size pattern and location, are selected appropriately, the destabilization process leads to tip vortex breakdown, and consequently to TV mitigation. The extra friction introduced by the roughness and the pressure variation on the blade normally lead to performance degradation (Johnsson and Ruttgerson 1991, Kruger et al. 2016, Asnaghi et al 2019(a)). As a result, practical application of roughness for TV mitigation strongly depends on minimizing this degradation, which can be achieved by optimizing the roughened area. This, however, requires detailed knowledge on where and how

*urban.svennberg@km.kongsberg.com

the tip vortex is initiated and develops.

In order to develop an analogy that can determine effective areas in TV formation and development, two cases are studied, an elliptical foil and a model scale propeller. The vortex structures around the elliptical foil resemble the propeller tip vortex behaviour while making it possible to be tested and evaluated in more detail. The tip vortex at the selected operating conditions is relatively stationary (Pennings et al. 2015(a), Pennings 2016) which reduces the computational requirements. The selected propeller is from a Kongsberg research series of highly skewed propellers having a low effective tip load and is typical for yachts and cruise ships, where it is very important to suppress and limit propeller-induced vibration and noise. For this type of propellers, the main source of noise and vibration is the vortex cavitation in the tip region. In our previous studies, numerical simulations of tip vortex flows around this propeller having smooth blades were carried out and successfully compared with experimental measurements (Asnaghi et al. 2018(a)). The analysis includes both numerical results and experimental measurements which are conducted in the cavitation tunnel at the Hydrodynamics Research Centre of Kongsberg Maritime Sweden AB, Kristinehamn, Sweden.

Implicit LES (ILES) is employed to solve the flow field and turbulence around the foil. The analysis of the propeller includes simulations at different operating conditions with different blade surface specifications. Since the open water condition and uniform inlet flow field are considered, RANS is employed to lower the computational cost of propeller simulations. All the simulations are carried out using OpenFOAM on appropriate grid resolutions for tip vortex propagation, at least 32 cells per vortex diameter according to previous studies guidelines (Asnaghi 2018, Asnaghi et al. 2020). In the propeller simulations, a curvature correction method, the η_3 model, is incorporated with the SST $k-\omega$ model to prevent overprediction of turbulent viscosity in highly swirling tip regions (Arolla 2013, Arolla and Durbin 2013).

The roughness is included in the simulations by employing two different approaches. In the first approach, a rough wall function is used to mimic the effects of roughness by affecting the turbulent properties in roughed areas based on the non-dimensionalized roughness height (Tapia 2009). This demands for having a wall-normal resolution larger than the roughness height. The second approach modifies the mesh topology by removing cells in roughed areas to create random roughness elements. While the first approach models the roughness effects, the second one includes approximately the roughness geometries into the simulations.

As mentioned earlier, the main challenge in practical applications of roughness in TV mitigation is finding an optimized roughness pattern that can give a reasonable balance between performance degradation and TV mitigation. To find this pattern, it is very crucial to know which areas close to the foil or blade surface provide the momentum of the TV either in the initiation step or its roll-up step. Therefore, as a first step for each case, the smooth condition is simulated and flow properties are evaluated with special focus on the TV properties.

The effective areas on the foil or the blade that contribute to the main TV are determined based on the Q-criterion, flow streamlines and pressure distribution. Then, different roughness patterns and arrangements are created from these effective areas to investigate how roughness application on them would affect the TV mitigation and performance degradation.

The experimental measurements are conducted to support the numerical analysis by providing the detailed TV core velocity distribution, high speed video recordings of TV flow in cavitating and inception conditions, and forces variations for different surface conditions of the foil. The analysis provides further knowledge on how roughness changes the flow pattern around the tip and mitigates cavitation inception.

In this study, the pressure minimum criterion is employed as an indication of cavitation inception. The results show that when the roughness pattern is optimized the cavitation number for TVC inception, σ_i, can be reduced by 35% with performance degradation of 1% in the elliptical foil case compared to its smooth surface condition. For the propeller over different operating conditions and compared to its smooth surface case, the averaged TVC inception improvement of 21% with performance degradation of 1.5% are noted.

EQUATIONS

The low pass filtered equations of mass and momentum are employed to model the flow field in the LES approach,

$$\frac{\partial \rho_{\mathrm{m}}}{\partial t}+\frac{\partial(\rho_{\mathrm{m}}\bar{u}_i)}{\partial x_i}=0 \tag{1}$$

$$\frac{\partial(\rho_{\mathrm{m}}\bar{u}_i)}{\partial t}+\frac{\partial(\rho_{\mathrm{m}}\bar{u}_i\bar{u}_j)}{\partial x_j}=-\frac{\partial \bar{p}}{\partial x_i}+\frac{\partial}{\partial x_j}(2\mu\bar{S}_{ij}-B_{ij})+\rho_{\mathrm{m}}g_i. \tag{2}$$

In Implicit LES, no explicit model is employed to compute the subgrid stress tensor, $B_{ij}=\rho(\overline{u_iu_j}-\bar{u}_i\bar{u}_j)$, and instead the numerical dissipation is considered enough to mimic the action of B_{ij} (Bensow and Fureby 2007, Bensow and Bark 2010).

The propeller open water condition with an uniform inlet velocity provide the possibility of modelling the flow in the steady state condition using RANS. For this case, the SST $k-\omega$ model with a curvature correction (CC) model is chosen (Asnaghi 2019(b)). In the selected CC model, the production term of the ω equation is multiplied by F_{rc},

$$F_{rc}=1+\alpha_1 \mid \eta_3 \mid +3\alpha_1\eta_3, \tag{3}$$

where $\alpha_1=-0.2$ and $C_r=2.0$. The non-dimensional strain rate and rotational rate tensors are used to compute the velocity gradient invariant η_3 (Arolla 2013),

$$\eta_1=\bar{S}^*_{ij}\bar{S}^*_{ij},\quad \eta_2=\bar{\Omega}^*_{ij}\bar{\Omega}^*_{ij},\quad \eta_3=\eta_1-\eta_2, \tag{4}$$

$$\bar{S}^*_{ij}=\tau\bar{S}_{ij},\quad \bar{\Omega}^*_{ij}=\tau\bar{\Omega}^{mod}_{ij}. \tag{5}$$

In order to normalize the tensors, the turbulent time scale τ is applied,

$$\tau = \max(\tau_1, \tau_3), \tag{6}$$

$$\tau_1 = \frac{1}{\beta^* \omega}, \quad \tau_2 = 6\sqrt{\frac{\nu}{\beta^* k\omega}}, \quad \tau_3 = (\tau_1^n \tau_2)^{\frac{1}{n+1}}, \tag{7}$$

with $n = 1.625$.

The modified rotational rate tensor incorporating the streamline curvature and frame rotation is,

$$\bar{\Omega}_{ij}^{mod} = \bar{\Omega}_{ij} + \Omega_{ij}^F + (C_r - 1)W_{ij}^A, \tag{8}$$

where $C_r = 2$ and Ω_{ij}^F represents the frame rotational tensor calculated from $\Omega_{ij}^F = -\epsilon_{ijk}\Omega_k^F$. Here, Ω_k^F is the angular frame velocity about the x_k-axis. The W_{ij}^A tensor which associates the effects of curvature corrections in the rotational rate tensor is defined by,

$$W_{ij}^A = -\epsilon_{ijk} B_{km} \bar{S}_{pr} \frac{D\bar{S}_{rq}}{Dt} \epsilon_{pqm}, \tag{9}$$

$$B_{km} = \frac{II_S^2 \delta_{km} + 12III_S \bar{S}_{km} + 6II_S \bar{S}_{kl}\bar{S}_{lm}}{2II_S^3 - 12III_S^2}, \tag{10}$$

$$II_S = \bar{S}_{kl}\bar{S}_{lk}, \quad III_S = \bar{S}_{kl}\bar{S}_{lm}\bar{S}_{mk}, \tag{11}$$

where $\frac{D\bar{S}_{rq}}{Dt}$ is the material derivative of the strain rate tensor. Please refer to Wallin & Johansson (2002) and Arola (2013) for further information.

For the simulations where roughness is modelled, the wall function developed by Tapia (2009) is employed,

$$u^+ = \frac{1}{\kappa}\ln(Ey^+) - \Delta B, \tag{12}$$

with $\kappa = 0.41$, $E = 9.8$, $y^+ = u_\tau y/\nu$, and the velocity shift correction ΔB due to the roughness elements. In this model, the nondimensional roughness height is presented by $K_s^+ = u_\tau K_s/\nu$ where K_s is the roughness average height, $u_\tau = \sqrt{\tau_w/\rho}$ is the shear velocity, and τ_w is the wall shear stress.

In our previous studies, the optimum roughness height for the studied cases that provides a reasonable balance between TVC mitigation and performance degradation is found to be K_s^+=35 (Asnaghi et al. 2019(a) and Asnaghi et al. 2019(c)). For this roughness height, the velocity correction term reads,

$$\Delta B = \frac{1}{\kappa}\ln\left[\frac{K_s^+ - 2.25}{87.75} + C_s K_s^+\right]\sin\big(0.425[\ln(K_s^+) - 0.811]\big). \tag{13}$$

In the selected wall function, shape and form of roughness elements are incorporated into the modelling through the C_s coefficient. However, there is no clear guideline to adjust this coefficient. It is suggested that it varies from 0.5 to 1 where C_s=0.5 corresponds to the uniformly distributed sand grain roughness. If the roughness elements deviate from the sand grains, the constant roughness should be adjusted by comparing the results with experimental data. The current simulations are performed by using C_s=0.5.

To identify vortical structures in the flow, the Q-criterion representing the local balance between shear strain and rotational tensor magnitudes, is employed (Hunt et al. 1998, Kolar 2007),

$$Q = \frac{1}{2}(\bar{\Omega}_{ij}\bar{\Omega}_{ij} - \bar{S}_{ij}\bar{S}_{ij}), \tag{14}$$

where the strain rate and rotational rate tensors are defined by,

$$\bar{S}_{ij} = \frac{1}{2}\left(\frac{\partial \bar{u}_i}{\partial x_j} + \frac{\partial \bar{u}_j}{\partial x_i}\right), \quad \bar{\Omega}_{ij} = \frac{1}{2}\left(\frac{\partial \bar{u}_i}{\partial x_j} - \frac{\partial \bar{u}_j}{\partial x_i}\right). \tag{15}$$

To simplify the cavitation inception detection, the minimum pressure criterion is employed (Asnaghi et al. 2018(b)),

$$\sigma_i = -C_{p,min}. \tag{16}$$

The hydrodynamic performance of the propeller is defined by using the non-dimensional thrust and torque coefficients, and the advance ratio,

$$K_T = \frac{T}{\rho n^2 D^4}, \quad K_Q = \frac{Q}{\rho n^2 D^5}, \quad J = \frac{V_A}{nD}. \tag{17}$$

In these equations, D is the propeller diameter, n is the rotational speed of the propeller in rev/sec, ρ is the fluid density, T is the propeller thrust force, Q is the propeller shaft torque, and V_A is the mean inflow velocity towards the propeller plane.

CASES DESCRIPTION

As mentioned earlier, two cases are considered to evaluate the impact of roughness on TV and to gain the insights on how and where the roughness should be applied in order to have a reasonable balance between TV mitigation and performance degradation. Following, the description of these cases, generated computational grids, and tested operating conditions are presented.

Case 1: Elliptical foil

The geometry of the foil is an elliptical planform having the NACA $66_2 - 415$ cross section with the root chord length C_0 = 0.1256 m. The projected surface area of the foil on the streamwise plane computed from the CAD file is A=0.01465 m^2 where coefficients such as lift and drag are calculated based on this area, $C_l = L/(0.5\rho U_{inlet}{}^2 A)$ and $C_d = D/(0.5\rho U_{inlet}{}^2 A)$. The foil has a half span of 150 mm, so that the tip is positioned in the centre of the test section (Schot et al. 2014, Pennings 2016). The computational domain of the foil, which mimics the TU Delft cavitation tunnel dimensions, is presented in Figure 1. Note that in this figure, the sizes are presented based on the foil root chord length.

The foil simulations are conducted at the angle of attack equal to 9 degrees and a constant inlet velocity of 6.8 m/s. In Figure 2, distribution of computational cells is presented. According to our findings, at least 32 grid points across the vortex diameter is required to predict a tip vortex flow in its near field region (Asnaghi 2018, Asnaghi et al. 2020). This corresponds to cell sizes equal to 0.0625

mm in the simulated condition. Close to the tip, two different refinement regions are defined, a refinement box covering the tip which is named Tip region refinement and two cylindrical shape refinement regions which are called Tip vortex trajectory refinement as presented in Figure 2a. The isotropic cell resolution of 0.0625 mm is applied in the Tip region refinement box and for the trajectory refinement anisotropic refinement resolution of 0.0625 mm in the in-plane section and 0.125 mm in the streamwise direction are employed. The baseline mesh resolution on the foil surface has both x^+ and $z^+ < 250$, but considerably finer in the refined tip region. The streamwise mesh distribution around the foil is presented in Figure 2b.

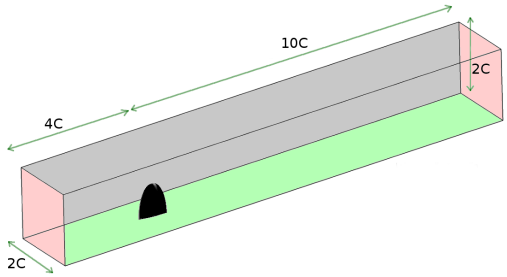

Figure 1: Computational domain of the foil simulations.

Two different wall normal resolutions are considered. In Mesh (I) which is prepared for modelling the roughness via the wall function, the wall normal resolution is $y^+ = 35$, and in Mesh (II) which is prepared for resolving the flow around the roughness elements, the wall normal resolution is $y^+ = 3$; Table 1.

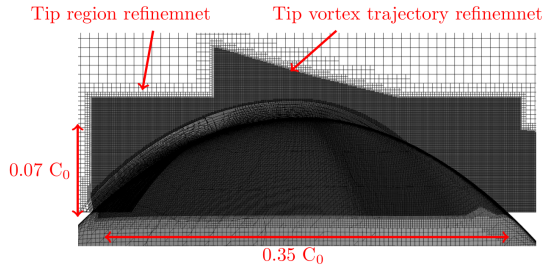

(a) Tip zoomed view

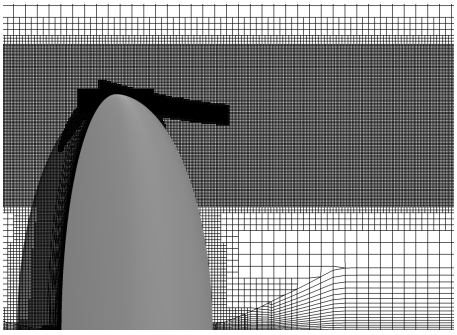

(b) Streamwise mesh distribution

Figure 2: Mesh distribution around the foil.

Table 1: Mesh specifications of the elliptical foil.

Mesh	y^+	Cells (M)	In-plane/streamwise resolution (mm)
(I)	35	31.8	0.062, 0.125
(II)	3	35.4	0.062, 0.125

The simulation of resolving flow around roughness elements is limited to the case with the optimum roughness pattern. As the surface resolution at the tip region is much finer than the considered roughness height, each roughness element covers around 8 surface faces. Roughness elements are chosen in a way to roughly lead to a roughness surface concentration around 50 % of the considered area. In Figure 3, the roughness elements distribution is presented.

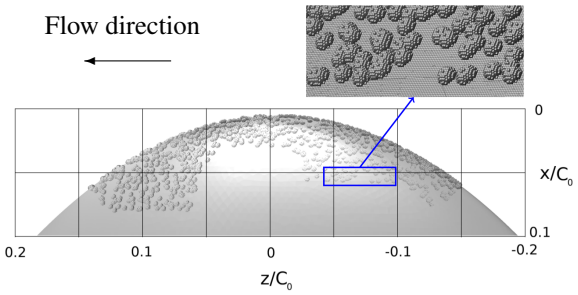

Figure 3: Roughness elements distribution in Mesh (II), tip zoomed view.

Case 2: High skewed propeller

The basic design of the propeller is from a research series of five-bladed highly skewed propellers having low effective tip load where it is very important to suppress and limit propeller-induced vibration and noise. In previous studies, the turbulence modelling impact, minimum required spatial mesh resolution and numerical set up for modelling propellers tip vortex flows in the near field region have been investigated (Svennberg et al. 2019, Asnaghi et al. 2018(a)). Here, the same guideline for the computational domain and mesh specifications is employed.

The computational domain used for the propeller is presented in Figure 4a. The domain is simplified to a cylinder extending 4D upstream the propeller and 8D downstream of the propeller where D=0.2543 m is the diameter of the propeller. The simulations are conducted at a constant inlet velocity , a fixed pressure outlet and the advance ratio is then set by adjusting the rotational rate of the propeller. No-slip wall boundary condition is used for the propeller and the shaft. The outer cylinder boundary is set as a slip boundary to reduce the mesh resolution requirements far from the propeller. In order to model the moving mesh, the computational domain has been decomposed into two regions connected to each other through AMI (Arbitrary Mesh Interpolation) boundaries. While the outer region is stationary, the rotation of the region close to the propeller where all interesting flow phenomena occur has been handled by MRF.

The baseline mesh resolution on the blades gives x^+ and $z^+ < 250$, with much finer resolutions at the leading edge and trailing edge of the blades due to the high geometry curvature. As the surface resolution close to the tip is determined by the tip refinement boxes, even finer resolution is achieved at the blade tip. The prismatic layers of the refined blade consist of 20 layers having extrusion factor of 1.15 where the first cell wall normal resolution is set equal to $y^+ = 35$ for wall modelling simulations, and equal to $y^+ = 5$ for resolving the flow around the roughness elements. As mentioned, the tip vortex refinement is applied on one blade only where three helical shape refinement zones are defined based on the primary vortex trajectory, Figure 4b. In Table 2, the operating conditions and normalised resolution details of the blade and tip vortex refinements are presented.

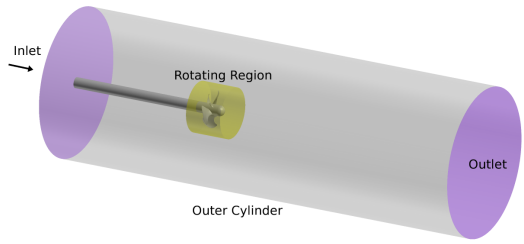

(a) Computational domain

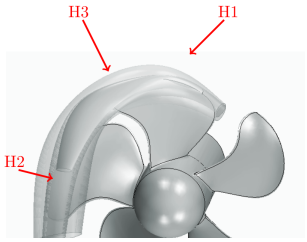

(b) Helical tip refinement

Figure 4: Mesh distribution of the model scale propeller.

Table 2: Operating conditions and mesh specifications of the propeller.

Propeller operating setup		
D(m)	U_{inlet} (m/s)	Re
0.2543	4.2	1.07×10^6
Blade surface resolution		
y^+	x^+	z^+
5, and 35	250	250
TV refinement resolution		
$H1^+$	$H2^+$	$H3^+$
40	20	10

At lower J values, e.g. J=0.82, the tip vortex forms on the back side of the blade either attached to the tip or slightly downstream. In our previous studies for mitigation of back side tip vortices (Asnaghi et al. 2019(c)), it is shown that a triangular region on the blade tip is the area where surface roughness have the most effect on TV formation. The application of roughness on these areas, illustrated in Figure 5, to mitigate back side TV is evaluated. At higher J values, e.g. J=1.26, the main vortex appears as a leading edge vortex formed on the front side of the blade. Therefore, the roughness pattern optimisation for this type of vortex focuses on finding important radial regions. In order to find which part of radial areas will have more impact on TV mitigation, smaller areas on the leading edge are considered, Figure 6. The summary of evaluated roughness patterns and their arrangements are presented in Table 3.

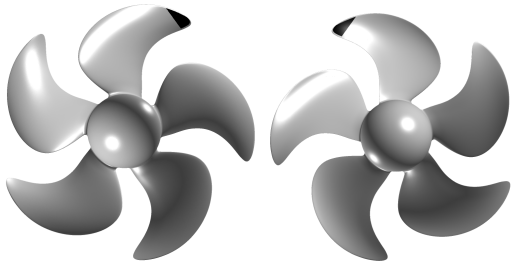

(a) Back side view **(b)** Front side view

Figure 5: Roughness areas coloured black on the back side and front side of the refined blade.

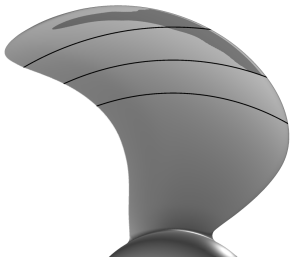

Figure 6: Radial leading edge roughness pattern RE80100 tested on the front side of the propeller.

Table 3: Summary of the roughness patterns tested on the back and front sides of the blade.

Pattern	**Where the roughness is applied:**
Smooth	The blade is smooth.
FS	Front side of the blade
BS	Back side of the blade
FR	Both sides of the blade (fully roughened)
BS Tip	Back side tip
FS Tip	Front side tip
BS + FS Tip	Tip of the back and front sides
RE8090	Front side leading edge in 0.8<r/R<0.9
RE8595	Front side leading edge in 0.85<r/R<0.95
RE90100	Front side leading edge in 0.9<r/R<1.0
RE80100	Front side leading edge in 0.8<r/R<1.0
ORP	Optimum roughness pattern BS Tip + RE80100

EXPERIMENTAL TESTS SETUP

The experiments are performed in the free surface cavitation tunnel at the Kongsberg Hydrodynamic Research Center, Kristinehamn, Sweden. The cross section of the test section is $0.8 \times 0.8\ m^2$ at the inlet and $0.8 \times 0.82\ m^2$ at the outlet. The height of the tunnel is extended gradually from inlet to outlet in order to compensate for the growth of the boundary layer and to facilitate a nearly zero-pressure gradient in the streamwise direction. This is provided by having the top plate horizontal and the bottom plate with a downward slope of 0.4 degrees where at the foil section, the vertical distance is about $0.81\ m$.

In order to test on a wider range of operating conditions, the experimental measurements are conducted on the foil having a uniform geometrical scale ratio of 2.398 compared to the elliptical foil tested at TU Delft (Pennings 2016, Pennings et al. 2015(b)). This leads to the root chord length $C_0 = 301.2\ mm$ and the span length of S=360 mm in the tested foil.

The measurements are performed with respect to the averaged free stream velocity ranging from 2.84 m/s to 4 m/s with typical fluctuations of $\pm 0.7\%$. The operating conditions were monitored during each experiment to prevent any deviations during the measurements. The dissolved oxygen concentration (DO) was used as a measure of the amount of dissolved gas in the water using a fluorescence-based optical sensor (Trioxmatic 690). It has a range of 0-600 % which equals to 0-60 $\frac{mg}{l}$ and the measurements were conducted at around 40 % corresponding to 4 $\frac{mg}{l}$. Our analysis clarifies that the free stream nuclei content is significant and the cavitation inception indications are in line with the week water condition of Arndt and Keller 1992.

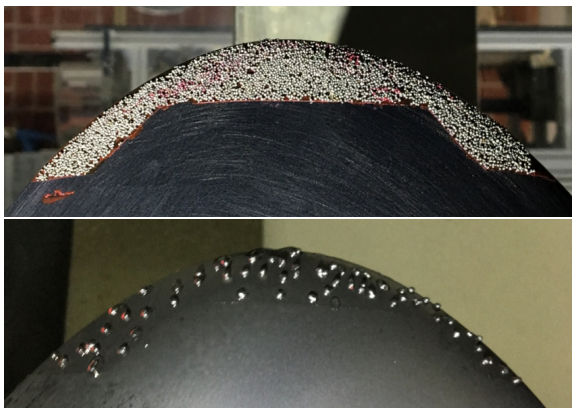

Figure 7: Distributions of sand grains on the foil suction side for one of the tested roughness patterns, tip zoomed view. Upper figure: uniform distribution (Exp. I), lower figure: randomly roughened spots (Exp. II).

To find the cavitation inception point, the outlet cavitation number has been varied by the steps of $\Delta\ \sigma = 0.1$. Around the cavitation inception point, high-speed recordings, which are 1 s long are used to find the lowest sigma where more than one occurrence of visible tip vortex cavitation can be observed. The measurements are conducted at the angle of attack (AOA) equal to 9 degrees where the inlet velocity is kept constant and the cavitation number is adjusted by changing the outlet pressure of the channel. Due to resource limitations, the roughness experimental tests are focused only on the roughness patterns, e.g. Figure 7, determined through the CFD analysis with the roughness height equal to 230 μm.

As presented in Figure 7, different methods of applying roughness on the foil surface are investigated in the experimental tests. In one approach, roughness elements are applied uniformly on the surface creating a uniform rough patch. This provides a suitable case for comparison with wall-modelled roughness of the numerical results. The second approach applies roughness elements locally, more like randomly placed larger roughness elements. This corresponds to the resolved roughness flow numerical results.

RESULTS

Elliptical Foil: tip vortex properties

In order to minimize the roughened area, it is necessary to determine regions of the flow or the foil that are important for the TV formation and development. Therefore, in the first step, the flow properties around the smooth foil is evaluated. In this regard, distribution of vortical structures and flow streamlines on both sides of the foil are investigated.

The Q-criterion iso-surface representing vortical structures, Figure 8, indicates a very little contribution from the pressure side, only in a small region on the top of the foil. On the suction side, vortical structures are formed more effectively on the leading edge, a region very close to the tip, and around the trailing edge. The trailing vortices are basically interacting with the low-pressure region of the tip vortex where the minimum tip vortex pressure usually occurs, i.e. $0.1 < z/C_0 < 0.2$.

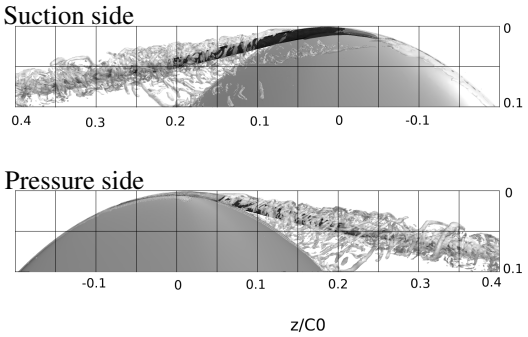

Figure 8: Distribution of the iso-surface Q=800 on the suction side and pressure side, smooth foil, tip zoomed view.

The flow streamlines passing through the tip vortex region, Figure 9, clarify that flow moves from the pressure side in $-0.15 < z/C_0 < -0.05$ to the suction side. This corresponds to the initiation of the vortex on the suction side in $-0.1 < z/C_0 < -0.05$. The figure highlights that the leading edge and the region very close to the tip on both suction side and pressure side are important regions in

the tip vortex development.

It is observed that most of the flow streamlines of the suction side leading edge form the tip vortex core rather than its outer region while the pressure side streamlines seem to feed both the vortex core and the outer region. As in the studied operating condition the tip vortex is formed on the suction side, the pressure side tip region seems to be less effective in feeding momentum into the vortex core.

Based on the discussion provided, it can be concluded that the main areas where roughness has impact on the tip vortex formation are the leading edge, the top region close to the tip of both sides, and the trailing region of the suction side. These areas are illustrated in Figure 10. According to this, different roughness patterns are arranged, Table 4, where the roughness distribution is assumed to be uniform, i.e. $C_s = 0.5$ in Eq. 13 with the roughness average height equal to 250 μm.

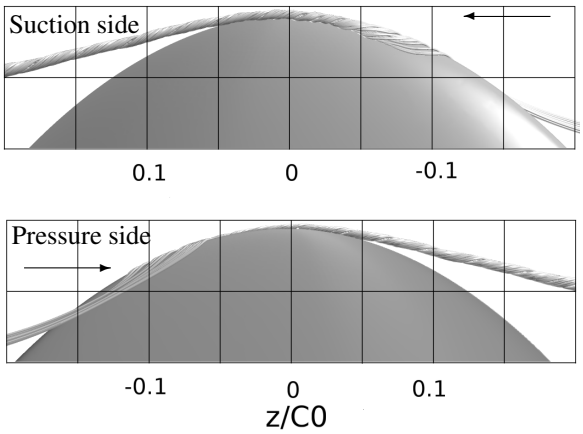

Figure 9: Flow streamlines passing through the vortex core, smooth foil, zoomed view.

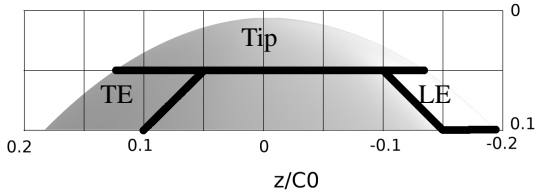

Figure 10: Foil effective areas in formation of tip vortex; leading edge (LE), trailing edge (TE), tip zoomed view of the suction side.

Table 4: Different patterns tested on the foil; SS: suction side, PS: pressure side, LE: leading edge, TE: trailing edge.

Case	(I)	(II)	(III)	(IV)
Roughness areas	SS Tip SS LE	PS Tip PS LE	SS Tip SS LE PS Tip PS LE	SS Tip SS LE SS TE

Elliptical Foil: roughness application

In Figure 11, the predicted cavitation inception of different roughness patterns is presented where numerical predictions and experimental measurements are illustrated by dashed bars and solid bars, respectively. Among the tested patterns, no obvious improvement is observed by the pattern (II) where the roughness is applied on the pressure side tip and leading edge. Other roughness patterns show considerable improvement in TV mitigation, especially pattern (IV) where the maximum mitigation is achieved. Moreover, a very good agreement between the numerical results and the experimental measurements is observed. It is known that the tip vortex can be sensitive to small variations in the flow and water quality and the sensitivity to turbulence modelling, inlet turbulence and water quality are therefore investigated and discussed in previous publications (Asnaghi 2018, Asnaghi et al. 2020).

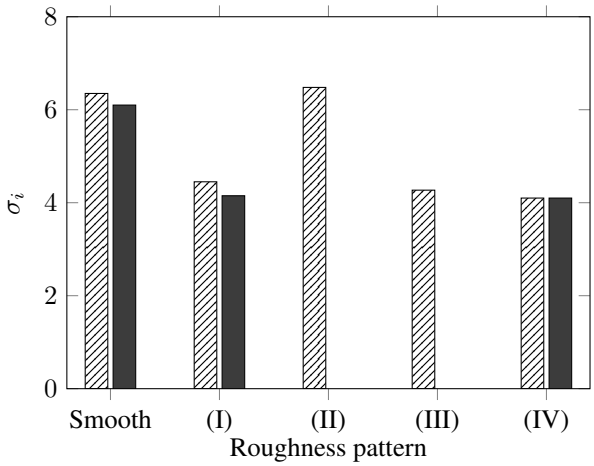

Figure 11: Cavitation inception versus different surface roughness patterns presented in Table 4, solid bars are the experimental measurements and dashed bars are the numerical predictions.

Table 5: Drag and lift forces results for different roughness patterns applied on the foil. The results are normalised by the smooth foil condition.

Case	Numerical results		Experimental data	
	$C_d(\%)$	$C_l(\%)$	$C_d(\%)$	$C_l(\%)$
(I)	0.8	-0.04	1.44	0.27
(II)	10.5	-0.93	-	-
(III)	16.9	-1.51	-	-
(IV)	1.7	-0.07	1.0	-0.24
FR	85.7	-6.51	-	-

In Table 5, the lift and drag forces for the roughness patterns are presented. The results are normalized by the smooth foil forces in order to provide the percentage of variations. The results of the fully rough foil is also included in this table as the reference of the extreme performance degradation condition. Among the roughness patterns, the highest increased drag force is observed in the

case (III) where the roughness is applied on the leading edge and tip of the suction side and pressure side. The results clarify that having roughness only on the suction side, case (I) and (IV), are favourable in terms of the forces evaluation. The comparison with the experimental measurements shows a reasonably good agreement, and also indicates that the performance degradation is less than 1.44 % in the optimized roughness pattern. By mutual consideration of the cavitation inception and forces, the roughness pattern (IV) is selected as the optimum roughness pattern for TV mitigation in the elliptical foil case.

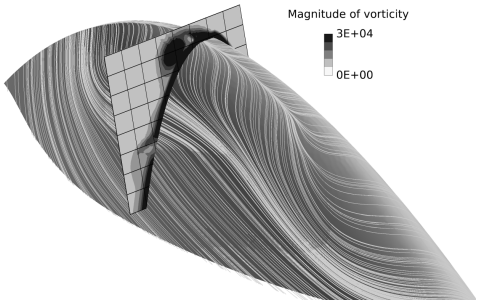

(a) Smooth

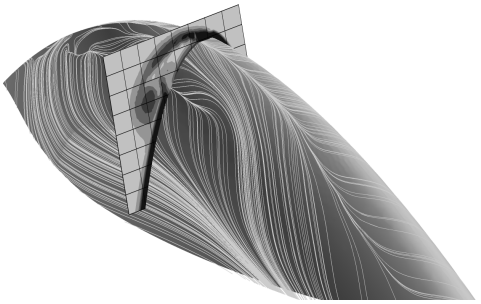

(b) Case (IV)

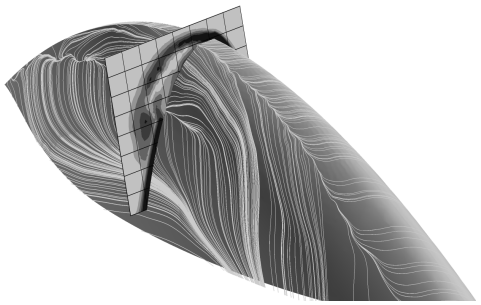

(c) Fully rough

Figure 12: Flow streamlines over the foil surface along with the vorticity magnitude distribution at $z/C_0 = 0$, isometric zoomed view of the suction side.

The flow streamlines over the foil surface for the smooth, roughness pattern (IV) and fully rough condition are presented in Figure 12. The vorticity magnitude distribution at $z/C_0 = 0$ is provided as an indicator of how the vortex strength is distributed. The flow streamlines over the foil highlight two separation lines located at the leading edge and the tip regions of the suction side in the roughness application, Figure 12b and Figure 12c. The separation line on the leading edge of the smooth condition, Figure 12a, is noted to happen later compared to the rough condition. The vorticity magnitude distribution clearly shows that in the smooth foil condition the tip vortex has the most concentrated momentum while application of roughness leads to lower angular momentum which is distributed over larger area.

The distribution of vortical structures for the cases of smooth, wall modelled roughness and resolved flow around the roughness elements is presented in Figure 13. As expected, when the flow around the roughness elements is resolved, finer flow structures are captured in the numerical simulations. An obvious difference between the flow structures of these three cases is the level of small structures surrounding the tip vortex. While both the smooth and wall modelled results show interactions of very fine small structures around the main tip vortex, the results of the resolved case shows lower amount of fine structures at that part. If it is believed these small structures around the main tip vortex are the products of the roll-up process, then the lower amount of structures around the tip vortex in the roughness resolved flow condition indicates that the roll-up process is the weakest in this condition. This, however, could not be captured by the wall modelling approach.

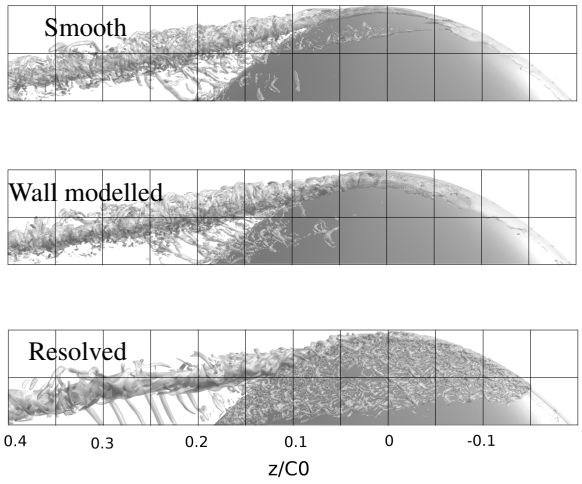

Figure 13: Distribution of the iso-surface Q=800 of the roughness pattern (IV) on the suction side, zoomed view.

In Figure 14, comparison of a snapshot of experimental observations and numerical results of resolving flow around roughness elements are presented. In the numerical results, the iso-surface of Q-criterion is used to represent vortical structures and an iso-surface of pressure to highlight TVC. It should be noted that the concentration of roughness elements used in the experimental test is lower than the one used in the numerical simulation. Even though, the comparison shows a general good agreement between numerical results and experimental observations in terms of the extent of TVC and its development.

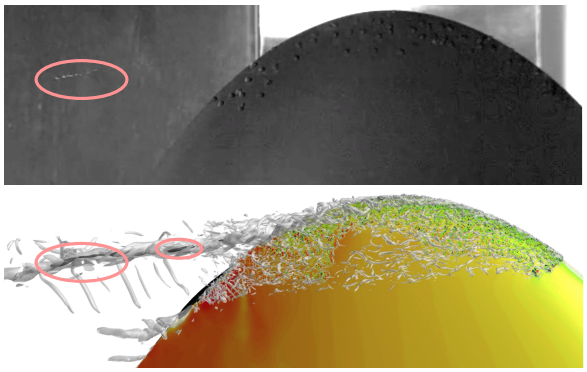

Figure 14: Comparison of TVC between numerical results and experimental observations, tip zoomed view of the suction side. TVC is distinguished by colored ovals.

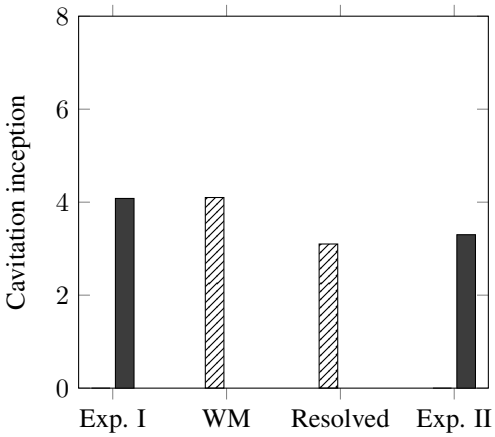

Figure 15: Cavitation inception prediction of the roughness pattern (IV) for different numerical modelling approaches versus the experimental measurement. Exp. I: tests on the uniform roughness sand distribution, Exp. II: tests on the randomly sparse distributions of roughness sand grains, WM:Wall modelled roughness simulations.

The tip vortex cavitation inception of the roughness pattern (IV) for different roughness modelling approaches are presented and compared with the experimental measurements in Figure 15. In this figure, Exp. I represents tests on the uniform roughness sand distribution and Exp. II indicates tests on the randomly sparse distributions of roughness sand grains. Therefore, Exp. I can be correlated to the numerical wall modelling approach where a uniform distribution of sand grains is assumed, and Exp. II can be correlated to the randomly distributed roughness elements and resolving approach. Both of the experimental measurements and numerical results predict a weaker tip vortex in the randomly distributed roughness elements condition. As discussed before, this can be related to having a weaker roll-up and also a more scattered vorticity distribution in this surface roughness condition compared to the uniform roughness distribution and its related wall modelled results. It can be noted that the general agreement between different roughness modelling approaches and their related experimental tests are satisfactory.

Numerical and experimental distributions of the vortex velocity for the smooth and case (IV) conditions are presented in Figure 16 and Figure 17. In each condition, the velocity is normalized by using the free stream velocity, i.e. U_{inlet}. By assuming that the vortex core center have zero rotational velocity, half of the distance between maximum and minimum tangential velocities is considered as the vortex radius. As can be seen, the tangential velocity presented in Figure 16 shows a very good agreement between numerical results and experimental measurements in the smooth and roughened conditions. Both the magnitude of the tangential velocity and its variation over vortex core are predicted reasonably good. This corresponds to an accurate prediction of angular momentum distributions in the simulations. Both of the numerical simulations and experimental measurements indicate that in the roughened surface condition the magnitude of the tangential velocity is decreased compared to the smooth condition.

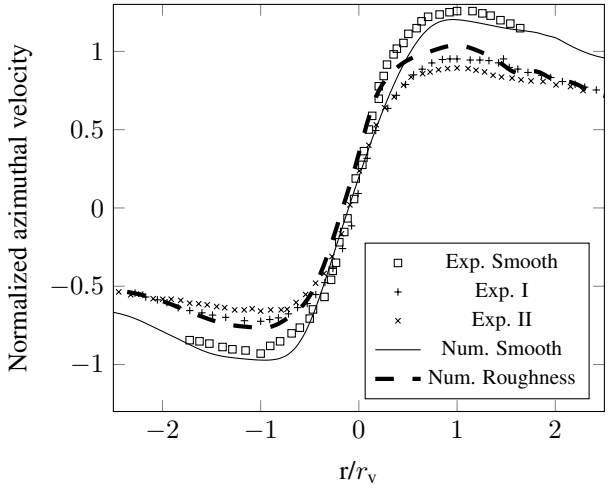

Figure 16: Normalized azimuthal velocity in the vortex core region at z/C_0=0.5 downstream of the foil tip.

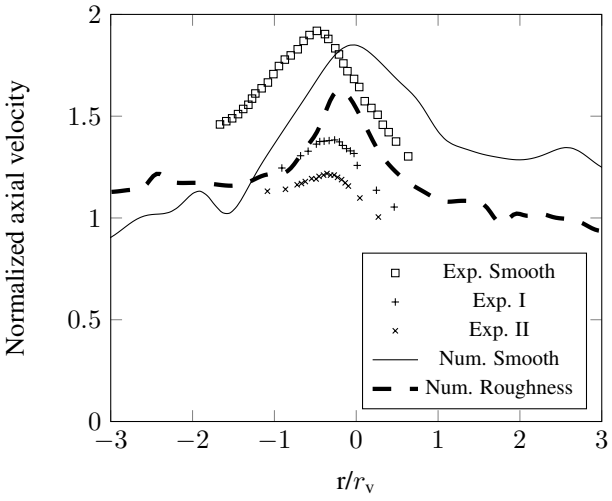

Figure 17: Variation of the normalized streamwise velocity in the vortex core region at z/C_0=0.5 downstream of the foil tip for the smooth and case (IV) surface conditions.

The vortex core axial velocity, i.e. streamwise velocity, shows more discrepancy between numerical results and experimental measurements. While in the numerical results the maximum axial velocity is predicted to happen relatively close to the vortex core center, the experimental measurements show the axial velocity peak happens slightly off the center, e.g. in the smooth condition it happens at r/r_v=0.5.

In the experimental tests, no obvious indication of increasing the risk of bubble or sheet cavitation on the foil by having roughness elements is observed. This is analyzed in both TVCI condition and also in developed TVC. In Figure 18, the time averaged cavitating tip vortex on the foil at σ=2.6 for different surface conditions is presented. The observations clearly show that in the smooth condition the tip vortex is stronger than the cases with roughness applications. Moreover, it can be observed that in the case (IV), TVC is slightly thinner than in the case (I) indicating a weaker TV in the case (IV).

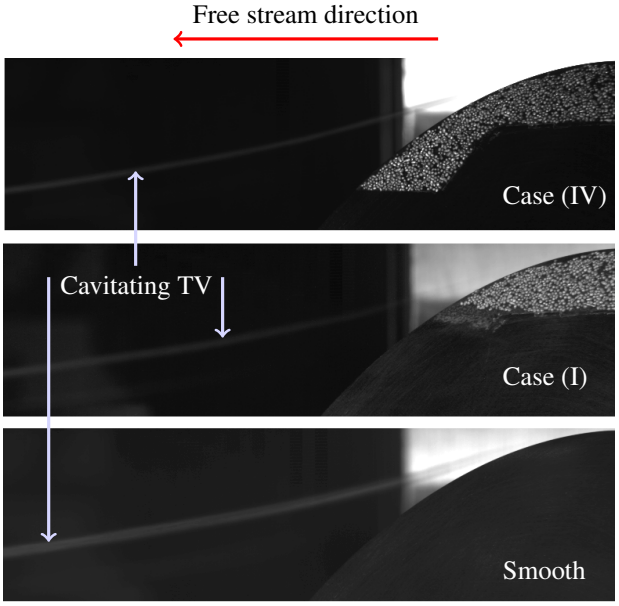

Figure 18: Time averaged cavitating tip vortex on the foil with and without roughness, σ=2.6, zoomed view of the suction side tip.

Propeller: tip vortex properties

The flow properties at a low J value where the tip vortex forms on the back side of the blade are presented in Figure 19. In this figure, the tip vortex is presented by the pressure iso-surface, the flow streamlines are presented by white lines over the blade surface, and the blade surface is coloured by the pressure coefficient distribution. The lower J values correspond to higher propeller rotational speeds which lead to a stronger tip vortex on the back side.

The flow streamlines clearly indicate that the flow is concentrated towards the tip of the blade, especially close to the trailing edge in 0.9<r/R<0.95 on the back side, where R is the propeller radius. This indicates a region proving momentum into the TV from the blade tip. On the front side, no obvious concentrated streamlines are observed. It seems that the flow streamlines from the front side evenly contribute to the tip vortex roll-up downstream of the tip rather than where the tip vortex originates.

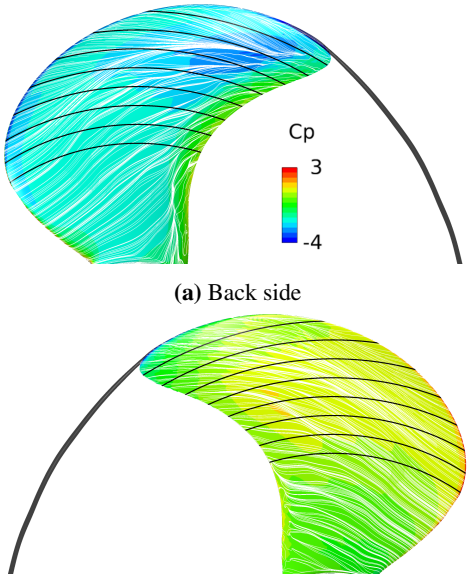

(a) Back side

(b) Front side

Figure 19: Flow properties for a back side tip vortex condition, J=0.82. The blade surface is coloured by C_p, the flow streamlines are presented in white, the tip vortex is presented by the pressure iso-surface equal to $C_p = -4$ coloured in black. The blade surface is divided by r/R=0.05.

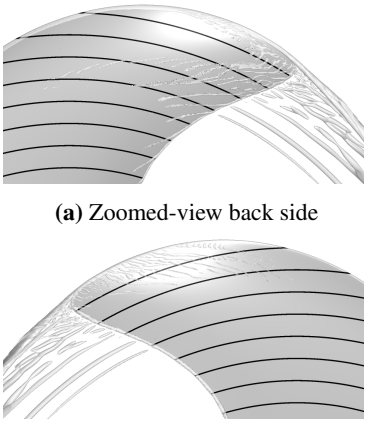

(a) Zoomed-view back side

(b) Zoomed-view front side

Figure 20: Distribution of Q-criterion iso-surface = 200 around the blade tip at J=0.82.

The distribution of vortical structures is presented by the iso-surface of Q-criterion equal to 200 in Figure 20. In 0.9<r/R<1.0 on the blade back side, the vortical structures appearing a triangular area which corresponds to the area where concentrated flow streamlines enter the TV. Based on the flow properties analysis of J=0.82, triangular areas on the back side and front side of the blade are

considered as important areas in the formation of the back side tip vortex. These areas are presented in Figure 5. The flow properties at J=1.26 where the tip vortex forms as a leading edge vortex are presented in Figure 21. At this operating condition, the leading edge vortex forms at lower radii, e.g. r/R=0.7, leading to an obvious flow suction into the vortex region which can be noted from concentrated flow streamlines on the front side in r/R<0.6. This corresponds to the vortices formed on the blade in this region, Figure 22. Interaction of these vortices on the leading edge defines the pressure distribution and TV location. Moreover, the results show that the trailing vortices shed from both back side and front side contribute to the tip vortex structures especially after leaving the blade.

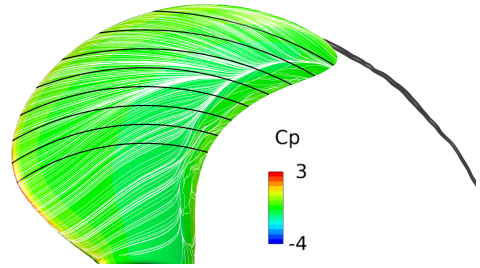

(a) Back side

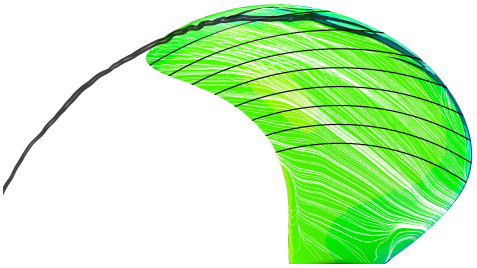

(b) Front side

Figure 21: Flow properties at J=1.26. The blade surface is coloured by C_{p}, the flow streamlines are presented in white, the tip vortex is presented by the pressure iso-surface equal to $C_{\mathrm{p}} = -2$ coloured in black.

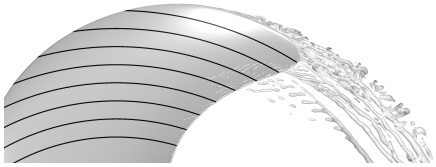

(a) Back side

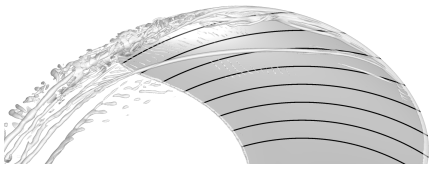

(b) Front side

Figure 22: Distribution of Q-criterion iso-surface = 200 around the blade tip at J=1.26.

These results clarify the effect of flow structures formed in 0.7<r/R region on the leading edge vortex strength and its development. Therefore, different roughness arrangements are considered for mitigation of the front side tip vortex based on radial distances and pressure distribution, Figure 6. The summary of these arrangements and their brief descriptions are presented in Table 3.

Propeller: roughness application

The cavitation inception prediction of different roughness patterns designed for the back side TVC at J=0.82 is presented in Figure 23. As mentioned earlier, at this operating condition the tip vortex is formed on the back side of the blade. The predicted cavitation inception in the BS tip and BS+FS tip patterns are close to each other, and the difference between them is believed to lie in the uncertainty of the numerical results in the current simulations. This indicates a little improvement in TV mitigation by having roughness on the FS tip when TV is formed on the BS.

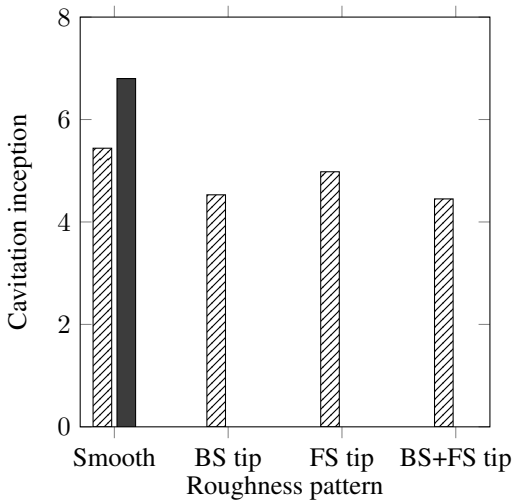

Figure 23: Variation of the cavitation inception versus different surface roughness patterns at J=0.82, solid bar is the extrapolated experimental measurements for the smooth blade. BS (back side) and FS (front side) patterns are presented in Figure 5.

Performance of the propeller including thrust, torque and open water efficiency for different roughness patterns are presented in Table 6. In order to clarify how these parameters change with respect to the blade smooth condition at J=0.82, they are normalized with the smooth propeller results. Having roughness on BS tip leads to a lower K_T around -0.8 % with a slightly higher required torque coefficient, K_Q, increase of 0.2 %. This results in a η_0 drop of 1.0 %. Having roughness on the FS tip, however, leads to higher K_T but it also requires a higher K_Q eventually resulting in a lower propeller efficiency, around -2.5 %. Further quantitative justification of these results demands uncertainty analysis which has been postponed for future studies.

Table 6: Variation of thrust, torque and efficiency relative to the smooth foil condition for different roughness patterns. BS: back side, FS: front side.

Case	K_T (%)	K_Q (%)	η_0 (%)
Smooth	–	–	–
BS tip	-0.8	0.2	-1.0
FS tip	1.2	3.8	-2.5
BS+FS tip	2.1	4.6	-2.4

The results, however, clearly confirm that the negative effects of roughness on the propeller performance is limited when the roughened area is limited. Even though the TVC mitigation of BS+FS tip pattern is slightly higher, because of having much lower performance degradation, the BS tip pattern is selected as the optimum roughness pattern for the back side TVC.

The roughness area optimization of the front side tip vortex is conducted at J=1.26. The flow structures on the back side are noted to affect the tip vortex properties especially downstream the tip when the trailing vortices interact with the tip vortex. However, very little improvement in TVC mitigation is observed when the roughness is applied on the BS of the blade compared to the smooth condition, while the results of FS and FR conditions are found to be similar, Figure 24. This clearly indicates that in order to mitigate the front side TVC, roughness should be applied on the front side.

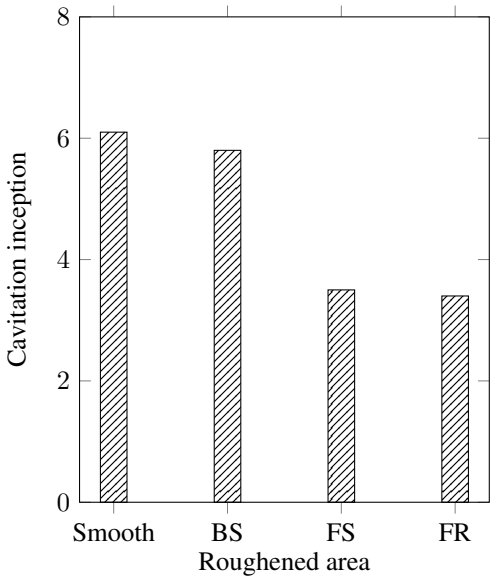

Figure 24: Variation of the cavitation inception versus different surface roughness areas at J=1.26, FR: fully rough foil, BS: back side roughness, FS: front side roughness.

Different criteria are tested to narrow down the areas where roughness have effect on the blade front side TV. Among the tested criterion, the combination of Q-criterion and pressure coefficient is found to be the most effective one. Based on this, different roughness patterns are created, Figure 6. The performance of these patterns relative to the smooth condition is presented in Table 7. It is observed that all of the patterns lead to higher K_T, K_Q, and even efficiency compared to the smooth condition. Contradictory to the back side roughness effects, in the front side tip vortex higher efficiency is gained by applying roughness. Although the uncertainty of numerical results can have an impact in this conclusion, it can be reasonably deduced that none of the patterns would have a negative impact on the propeller performance. As a result, the pattern that has the highest TVC mitigation is selected as the optimum roughness pattern for the front side TVC mitigation, i.e. RE80100.

Table 7: Variation of thrust, torque, efficiency and TVC inception relative to the smooth foil condition for different roughness patterns on the front side leading edge, J=1.26.

Case	K_T (%)	K_Q (%)	η_0 (%)	σ_i (%)
Smooth	–	–	–	–
RE8090	2.21	1.55	0.64	-22.2
RE90100	4.17	3.37	0.78	-20.3
RE8595	3.22	2.44	0.75	-29.1
RE80100	4.8	3.87	0.90	-35.2

Propeller: Optimum roughness pattern

Combination of the roughness patterns obtained for the back side tip vortex at J=0.82 and the front side leading edge vortex at J=1.26 is considered as the optimum roughness pattern that can be used over different operating conditions. In Figure 25, the open water performance of the propeller in the smooth and optimum roughness pattern (ORP) conditions is presented. In J <1.125, similar torque coefficients are predicted in smooth and ORP while the thrust coefficient is lower in ORP. For larger values of J, the produced thrust in smooth and ORP conditions are similar while more torque is needed in ORP condition. This leads to having a lower efficiency in ORP condition across all of the operating conditions. The trend of efficiency variation is found to be similar in smooth and ORP conditions.

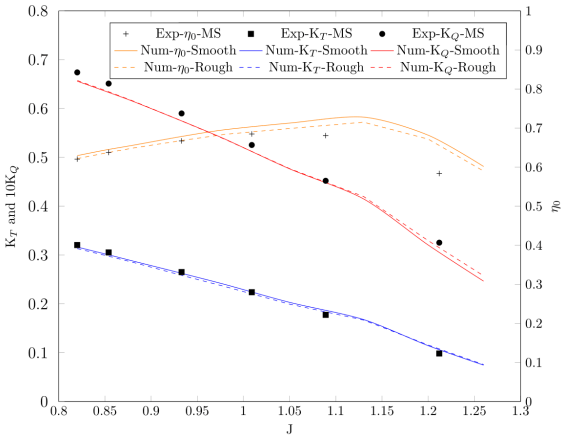

Figure 25: Comparison of the open water performance of the model scale propeller in the smooth and optimised roughness area conditions. Exp. data is for the smooth condition.

Detailed comparison of TVC mitigation and performance degradation is presented in Figure 26. The results of the propeller design operating condition, i.e. J=0.93, is included in this figure as well. It can be noted that the average performance degradation for ORP is around 1.5% and the average reduction of the cavitation number for TVC inception, σ_i, is 21%. The lowest impact of roughness on TVC mitigation is found to be at the bottom of the cavitation inception bucket around J=0.93 while the impact of roughness when the TVC is stronger is found to be larger.

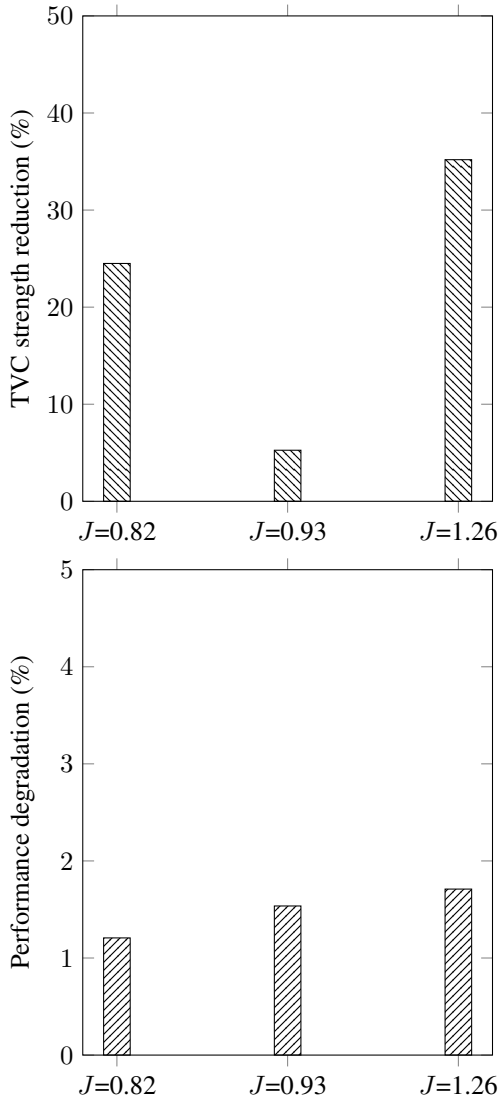

Figure 26: Optimum roughness pattern results of the propeller. TVC and propeller performance of each operating condition is normalised by the smooth propeller results of that condition.

CONCLUSIONS

The application of roughness to mitigate tip vortex (TV) strength is evaluated by using numerical and experimental analyses of the flow over an elliptical foil and a model scale propeller. The numerical investigations consist of LES results for the elliptical foil and RANS results, with the SST k-ω model, for the propeller. In each case, an appropriate resolution is employed to capture the TV; at least 32 grid points across the vortex diameter according to our previous findings. A curvature correction model is incorporated into the SST k-ω model to prevent the turbulent viscosity over prediction in the highly rotational regions. The roughness is included in the simulations by using two different approaches; employing a rough wall function and resolving the flow field around the roughness elements.

A series of experimental tests are conducted in the free surface cavitation tunnel at the Kongsberg Hydrodynamic Research Center, Kristinehamn, Sweden, to support the numerical analysis. Along with the force measurements, high-speed video recordings and LDV are employed to provide further details on the TV flow properties in different roughness pattern configurations.

The negative effects of roughness on the performance can be minimized by the optimization of roughened area by simultaneous consideration of TV cavitation suppression and the performance degradation. This is achieved by detailed analysis of the flow properties and structures effective in TV formation and development.

Based on the analyses of different flow criteria over the smooth condition, different roughness area configurations are created for the elliptical foil and the propeller. For each configuration, roughness application and its impact on the TV cavitation and the performance are evaluated to find the optimum roughness pattern.

For the elliptical foil, it is found that the optimum roughness pattern consist of areas on the leading edge, tip and trailing edge of the suction side. For the evaluated propeller design, two distinct types of tip vortices are observed. At lower advance ratio numbers, the vortex forms on the tip of the blade which can incept either on the tip or slightly downstream depending on the TV strength dependency on the roll-up process. For this type of TV, application of roughness on the blade tip region where the vortex forms is found to be effective. The other type of TV appears at higher J values as leading edge TV where roughness application on the limited area of leading edge on the same side of the vortex roll-up is found to be effective. The optimum pattern that can be used across different operating conditions are obtained by simultaneous application of roughness on these two areas.

The capability of using roughness to suppress the tip vortex cavitation (TVC) is proved by both the numerical results and experimental measurements. We show that for the elliptical foil the reduction of TVC inception number, σ_i, as large as 35 $\%$ with performance degradation less than 2 $\%$ compared to its smooth surface condition, and for the roughened propeller an average TVC inception reduction of 21% with an average performance degradation of 1.5% compared to the smooth propeller are achievable. Moreover, no indication of increasing the risk of bubble or sheet cavitation around the roughness elements is noted during the experimental tests. There are, however, several parameters such as wake flow effects, roughness impact on the

cavitating tip vortex conditions, and cavitation hysteresis that are left for future studies. Full scale simulations are ongoing and full scale tests will hopefully be conducted in the near future.

ACKNOWLEDGEMENTS

Financial support for this work has been provided by Vinnova through the RoughProp project, Grant number 2018-04085, and Kongsberg Maritime Sweden AB through the University Technology Centre in Computational Hydrodynamics hosted at the Department of Mechanics and Maritime Sciences at Chalmers. The simulations are performed on resources at Chalmers Centre for Computational Science and Engineering (C3SE) provided by the Swedish National Infrastructure for Computing (SNIC).

REFERENCES

Arndt, R.E.A., Arakeri, V.H. & H. Higuchi., "Some observations of tip-vortex cavitation," Journal of Fluids Mechanics, 229, 1991.

Arndt, R.E.A. & Keller, A., "Water quality effects on cavitation inception in a trailing vortex,". Journal of Fluids Engineering, 114(3), 430438, 1992.

Arndt, R.E.A., "Cavitation in vortical flows," Annual Review of Fluid Mechanics, 34:143175, 2002

Arolla, S.K., "Modeling and eddy simulation of rotating and curved turbulent flow," Doctoral Thesis, Iowa State University, Ames, Iowa, 2013.

Arolla, S.K. & Durbin, P.A., "Modelling rotation and curvature effects within scalar eddy viscosity model framework," Int. J. Heat Fluid Flow, 39 (1), 2013.

Asnaghi, A., "Computational modelling for cavitation and tip vortex flows," PhD thesis, Chalmers University of Technology, 2018.

Asnaghi, A., Svennberg, U. & Bensow, R.E., "Numerical and experimental analysis of cavitation inception behaviour for high-skewed low-noise propellers," Applied Ocean Research **79**(1), 2018 (a).

Asnaghi, A., Svennberg, U. & Bensow, R.E., "Analysis of tip vortex inception prediction methods," Ocean Engineering **167**(1), 2018 (b).

Asnaghi, A. Svennberg, U. Gustafsson, R. & Bensow, R.E., "Roughness Effects on the Tip Vortex Strength and Cavitation Inception," Sixth International Symposium on Marine Propulsors, Rome, Italy, May 2019 (a).

Asnaghi, A., Svennberg, U. & Bensow, R.E., "Evaluation of curvature correction methods for tip vortex prediction in SST k turbulence model framework," International Journal of Heat and Fluid Flow, 75, 2019 (b), pp 135-152.

Asnaghi, A., Svennberg, U., Gustafsson, R. & Bensow, R.E., "Propeller tip vortex cavitation mitigation using roughness," In Proceedings of VIII International Conference on Computational Methods in Marine Eng., MARINE 2019, Gothenburg, Sweden, 2019 (c).

Asnaghi, A., Svennberg, U. & Bensow, R.E., "Large Eddy Simulations of cavitating tip vortex flows," Ocean Engineering, 195, 2020.

Baily, S. & Tavoularis, S.,"Measurements of the velocity field of a wing-tip vortex, wandering in grid turbulence," Journal of Fluid Mechanics **60**(1), 2008.

Bensow, R.E. & Fureby, C., "On the justification and extension of mixed methods in LES," J. Turbulence **8**(1), 2007.

Bensow, R.E. & Bark, G., "Implicit LES predictions of the cavitating flow on a propeller," Journal of Fluids Engineering **132**(4), 2010.

Bosschers, J., "Propeller tip-vortex cavitation and its broadband noise," PhD thesis, University of Twente, 2018.

Higuchi, H., Arndt, R.E.A. & Rogers, M.F., "Characteristics of tip vortex cavitation noise," Journal of Fluids Engineering, Transactions of the ASME, 111(4):495501, 1989.

Hsiao, C.T. & Chahine, G.L., "Scaling of tip vortex cavitation inception noise with a bubble dynamics model accounting for nuclei size distribution," Journal of Fluids Engineering, Transactions of the ASME, 127(1):5565, 2005.

Hunt, J.C.R., Wray, A.A. & Moin, P., "Eddies, stream, and convergence zones in turbulent flows," Center for Turbulence Research Report CTR-S88, 1998.

Johnsson, C.A. & Ruttgerson, O., "Leading edge roughness: a way to improve propeller tip vortex cavitation," In Propeller Shafting Symposium, 1991.

Kolar, V., "Vortex identification: New requirements and limitations,"International Journal of Heat and Fluid, 28, 2007

Kruger, C., Kornev, N. & Greitsch, L., "Influence of propeller tip roughness on tip vortex strength and propeller performance," Ship Technology Research **63**(2), 2016.

Kuiper, G.,"Cavitation inception on ship propeller models," PhD thesis, Delft University of Technology, 1981.

Pennings, P.C., Bosschers, J., Westerweel, J. & Van Terwisga, T.J.C., "Dynamics of isolated vortex cavitation," Journal of Fluid Mechanics, 778:288313, 2015 (a).

Pennings, P.C., Westerweel, J. & van Terwisga, T.J.C., "Flow field measurement around vortex cavitation," Experiments in Fluids **56**(11), 2015 (b).

Pennings, P.C., "Dynamics of Vortex Cavitation," PhD thesis, TU Delft University, 2016.

Schot, J.J.A., Pennings, P.C., Pourquie, M.J.B.M. & van Terwisga, T.J.C., "Modelling of tip vortex cavitation for engineering applications in OpenFOAM," In 11th World Congress on Computational Mechanics, July 20-25, 2014, Barcelona, Spain.

Souders, W.G. & Platzer, G.P., "Tip vortex cavitation characteristics and delay of inception on a three dimensional hydrofoil,"

Naval Ship Research and Development Center,1981.

Svennberg, U., Ahl, D. & Asnaghi, A., "Tip vortex cavitation inception estimation at an industrial level," Sixth International Symposium on Marine Propulsors: smp19, Rome, Italy, May 2019.

Tapia, X.P., "Modelling of wind flow over complex terrain using OpenFoam," Master thesis, University of Gavle, 2009.

Vesting, F., Gustafsson, R. & Bensow R.E., "Development and application of optimisation algorithms for propeller design," Ship Technology Research, 63(1):5069, 2016.

Wallin, S. & Johansson, A.V., "Modelling streamline curvature effects in explicit algebraic Reynolds stress turbulence models," International Journal of Heat and Fluid Flow, 23(5):721 730, 2002.

Wijngaarden, E.V., Bosschers, J. & Kuiper, G., "Aspects of the cavitating propeller tip vortex as a source of inboard noise and vibration," Proceedings of FEDSM2005, ASME Fluids Engineering Division Summer Meeting and Exhibition, Houston, TX, USA, 2005.